Supporting Information for "Emerging impacts of enhanced Greenland melting on Labrador Sea dynamics"

Ilana Schiller-Weiss[1], Torge Martin[1], Franziska U. Schwarzkopf[1]

[1]GEOMAR Helmholtz Centre for Ocean Research Kiel, Kiel, Germany

Contents of this file

1. Text S1 to S5

2. Figures S1 to S5

Introduction

This supporting information includes the VIKING20X model description and complementing figures supporting the main text. In Addition to annual mean salinity and temperature in Figure 2, we here provide the winter and summer mean of surface salinity, temperature, and density anomalies in the subpolar North Atlantic (SPNA) (Text S1 and Figure S1). Text S2 and Figure S2 shows changes in the cumulative alongshore wind stress along the west Greenland shelf. The discussion on the current structure along the West Greenland Current (WGC) based on mooring locations is supported by Text and Figure S3, in which we present the temporal evolution of the mean WGC velocity and correlations between the current velocity and horizontal density gradient. Text and Figure S4 show the stratification and the Greenland meltwater passive tracer content percent change between the two model runs (REF and SENS) in 2009 and 2012, two years where deep convection was strong in the Labrador Sea (LAB) prior to the intensification of deep convection in both the east and west in 2015–2018 (de Jong & de Steur, 2016; Piron et al., 2016, 2017; Rühs et al., 2021). Text S5 and Figure S5 discuss the differences in convective

resistance (CR) between REF and SENS and the temporal evolution of CR over the potential deep convection area (pDCA).

VIKING20X model description

VIKING20X employs the NEMO3.6 ocean engine (Madec, 2016) and utilizes a two-way nesting with Adaptive Grid Refinement in Fortran (AGRIF) (Debreu et al., 2008) with a regional horizontally refined grid at 1/20° over the south and north Atlantic oceans (34°S–70°N) (see Figure 1 of (Biastoch et al., 2021)). The refinement permits the explicit simulation of mesoscale eddies (Hallberg, 2013), which improves the representation of deep convection in the LAB and Atlantic Meridional Overturning Circulation variability (Biastoch et al., 2021; Rühs et al., 2021). There needs to be adequate horizontal resolution particularly near the shelf to realistically simulate the impact from Greenland freshwater and role of mesoscale eddies therein (Gillard et al., 2016; Stolzenberger et al., 2022; Schiller-Weiss et al., 2023). The atmospheric forcing for both runs is JRA55-do (Tsujino et al., 2018) which includes estimates of Greenland freshwater fluxes provided as daily mean data and derived from monthly and spatially varying liquid runoff and solid discharge from Bamber et al. (2018) covering the period 1958–2016. The freshwater is released at the surface along the coastline and is tagged by a passive tracer.

The two model experiments, REF and SENS, are spun off from the hindcast VIKING20X-JRA-OMIP of Biastoch et al. (2021), which starts from rest in 1958 initialized with climatological hydrographic conditions of the World Ocean Atlas. Both experiments start from January 1997 and run through December 2021. To overcome numerical instabilities with the passive tracer occurring along some steep topography, a regionally confined no-slip lateral boundary condition has been introduced in a 0.5° × 0.5° box in the South-East corner of Cat Island, Bahamas. Besides this change, REF is identical to VIKING20X-JRA-OMIP until 2016. For the years

2017–2021 the Greenland freshwater fluxes, which lack interannual variability in JRA55-do, are scaled to match the variability reported by Slater et al. (2021). For this we computed a simple linear regression for the Greenland total annual mean freshwater flux of Bamber et al. (2018) using the respective runoff estimates of Slater et al. (2021).

Text S1

Figure S1 show the mean winter and summer sea surface salinity (SSS), temperature (SST), and potential density differences between REF and SENS over the period 2002–2021. There is a freshening along the east and west Greenland boundaries, particularly in summer when Greenland melting peaks (dark purple area around the shelf in Figure S1b). While there is cooling found along the Greenland shelf boundary in both seasons (Figure S1c, d), it is particularly strong in the very north of the Labrador basin towards Davis Strait (Figure S1c).

The red/cyan contours in Figure S1a, c, e mark the 15% sea ice concentration outline (i.e. the sea ice edge) in winter in REF/SENS, with REF sea ice coverage extending further south. Figure S1e, f show the winter and summer density differences. There is a strong seasonal cycle present with strong density and salinity differences along the Greenland boundary current in summer due to enhanced Greenland melt. Salinity appears to dominate the surface potential density with significantly lower differences found further offshore in winter (Figure S1a, e).
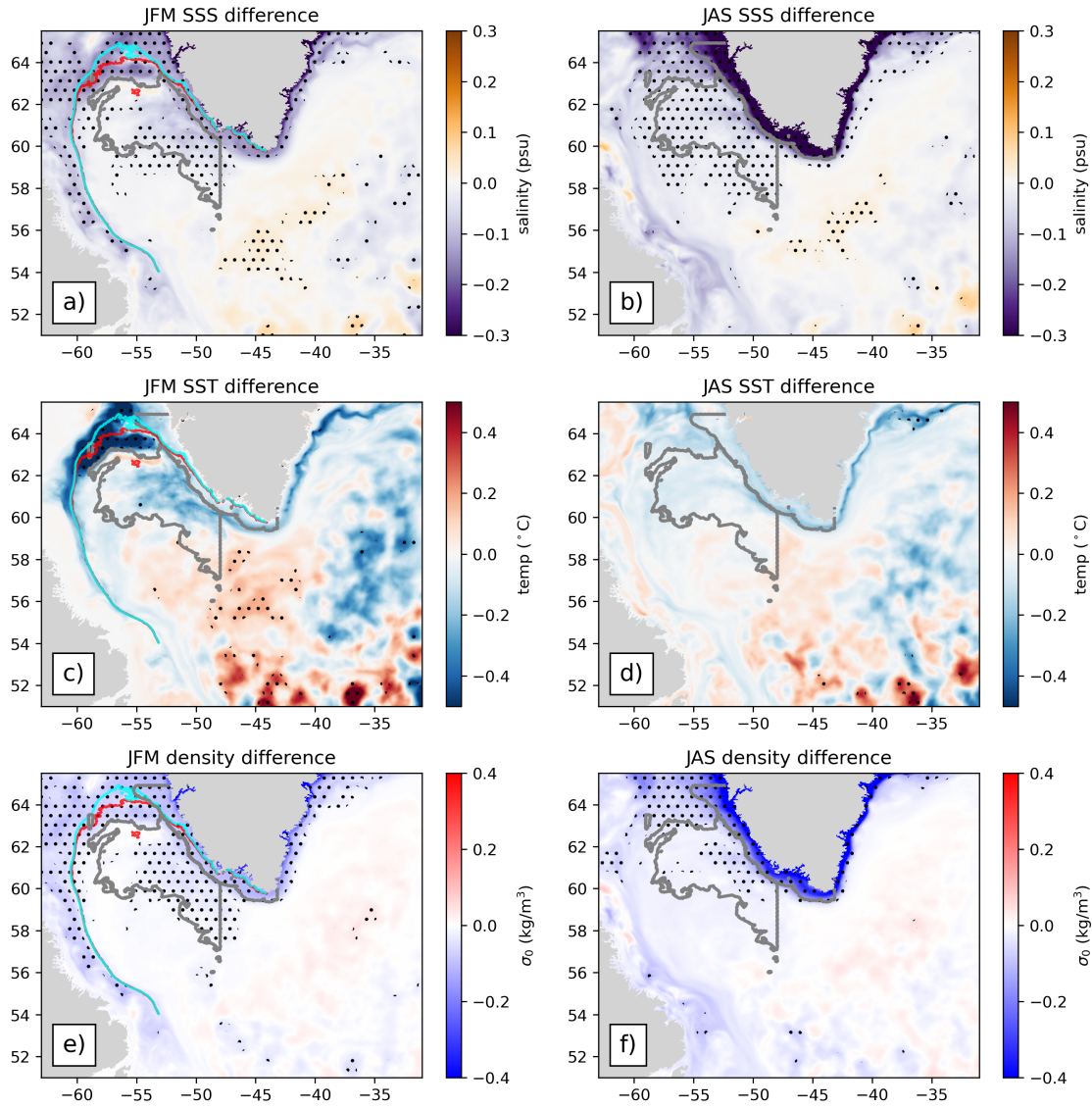
Figure S1. (a) Mean (2002–2021) winter (January–March) sea surface salinity (SSS) difference (REF minus SENS). (b) Mean summer (July–September) SSS differences. (c) Winter sea surface temperature (SST) difference. (d) Summer SST difference. (e) Winter surface potential density difference. (f) Summer potential density difference. Black stippling indicates statistically significant areas. Gray contours indicate the west Greenland shelf and eddy shedding region.

February 28, 2024, 2:28pm

Text S2

Figure S2 shows the cumulative alongshore wind stress from June–December averaged over the west Greenland shelf (gray contour along the shelf shown in Figure S1). Alongshore wind weakens in summer and increase in winter, where winds along west Greenland can be upwelling favorable and transport freshwater offshore (Castelao et al., 2019; Luo et al., 2016). As the wind stress shows strong instantaneous variability, computing the cumulative alongshore wind stress permits for substantial upwelling and downwelling favorable winters to be distinguished on an annual basis (Castelao et al., 2019). The cumulative alongshore wind stress is grouped into two categories of anomalous upwelling and downwelling favorable years (15th and 85th percentiles), shown in the blue (upwelling) and orange (downwelling) lines in Figure S2.

The summer of 2010 is where strong Greenland melting occurred (Tedesco et al., 2011). In the winter of 2010, winds were downwelling favorable where freshwater along the shelf is constrained to the coast and transported northward to Baffin Bay or follows the isobaths surrounding the LAB basin (Castelao et al., 2019).
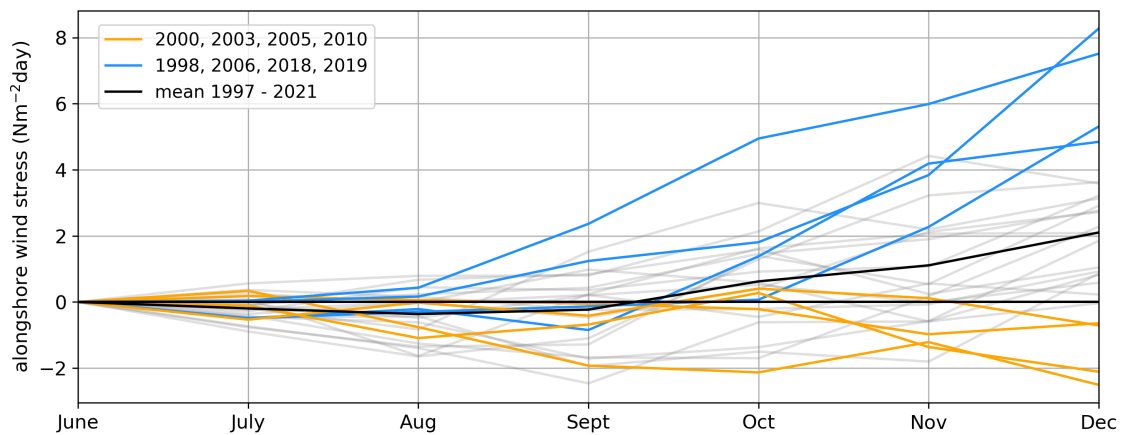

Figure S2. Cumulative alongshore wind stress from June–December averaged over the west Greenland shelf region. Black line indicates the mean alongshore wind stress, blue/orange lines indicate years with upwelling/downwelling favorable conditions outside the 15th/85th percentile.

February 28, 2024, 2:28pm

Text S3

The mean (2002–2021) West Greenland Current (WGC) velocity structure shown in Figure S3a. b, and c is taken over three repeat standard cross sections from the model output: OSNAP West (Lozier et al., 2019), Cape Desolation, and Fylla Bank (Mortensen, 2018; Myers et al., 2009). The current velocity magnitude along the OSNAP West section (Figure S3a) shows two peaks in the velocity at the shelf and just off the shelfbreak along the slope. The coastal current is present at Cape Desolation (Figure S3b) but slightly weaker than at OSNAP West.

The annual mean current speed for the coastal and slope current per cross section is shown in Figure S3d, e, f. It is at OSNAP West where the coastal and slope current strength in REF shows a significant increase compared to SENS (Figure S3d). At Cape Desolation, the coastal current for REF and SENS show the same variability where REF has slightly higher annual mean current velocities than SENS. However at the slope current, there is differing variability between the two runs. At Cape Desolation there are strong topographical differences and changes in alongshore wind stress that result in baroclinic instabilities (Gou et al., 2021, 2022; Pacini & Pickart, 2022), potentially explaining for the lack of coherent variability between REF and sensitivity run in the slope current (Figure S3e). The coastal current speed in REF is slightly greater than in SENS at Fylla Bank, and the slope current speeds are slightly greater in REF. The speed in the coastal current between the three cross sections decrease further north, while the slope current increases from OSNAP West to Cape Desolation and decreases at Fylla Bank.

We evaluate the correlation of the coastal and slope current velocities at each cross section with the local surface horizontal density gradient at each grid node in REF. The correlation maps between the coastal current velocity and density gradient for OSNAP West, Cape Desolation, and Fylla Bank are shown in Figures S3g, h, i. For all the cross sections, there are significant,

positive correlations between the density gradient and coastal current speed along the east and west Greenland shelves. There is a patch of negative correlations further offshore, showing a potential dipole pattern of near shelf changes in the density gradient suggesting an offshore meandering of the density front to be associated with a weaker coastal current.

Figure S3j, k, l show the same correlation but for the slope current velocity. For OSNAP West, there is a large patch of positive correlations in the eddy shedding region (Figure S3j), while for Cape Desolation there are positive correlations just off the section encircling the Labrador basin (Figure S3k). In contrast, for Fylla Bank, positive correlations are confined to the Greenland shelf (Figure S3l).

For a rather schematic illustration of the overall correlation between the boundary currents and the density gradient towards the LAB interior, we compute a "cumulative correlation". We first set a threshold by retaining only correlations that are statistically significant (areas defined by the gray contour based on 1st/99th percentiles), and then we compute the sum of all correlation maps from each section:

$$R_{all} = \sum_{n=1}^{N} R_n \ \text{ with } R_{all} \in [-1, 1], \tag{1}$$

where R_N is the evaluated correlation coefficient between the coastal and slope current velocity with the surface horizontal density gradient for N number of cross sections. As the sum will be greater than $|\pm 1|$, we cap the cumulative correlation coefficient R_{all} at ± 1.
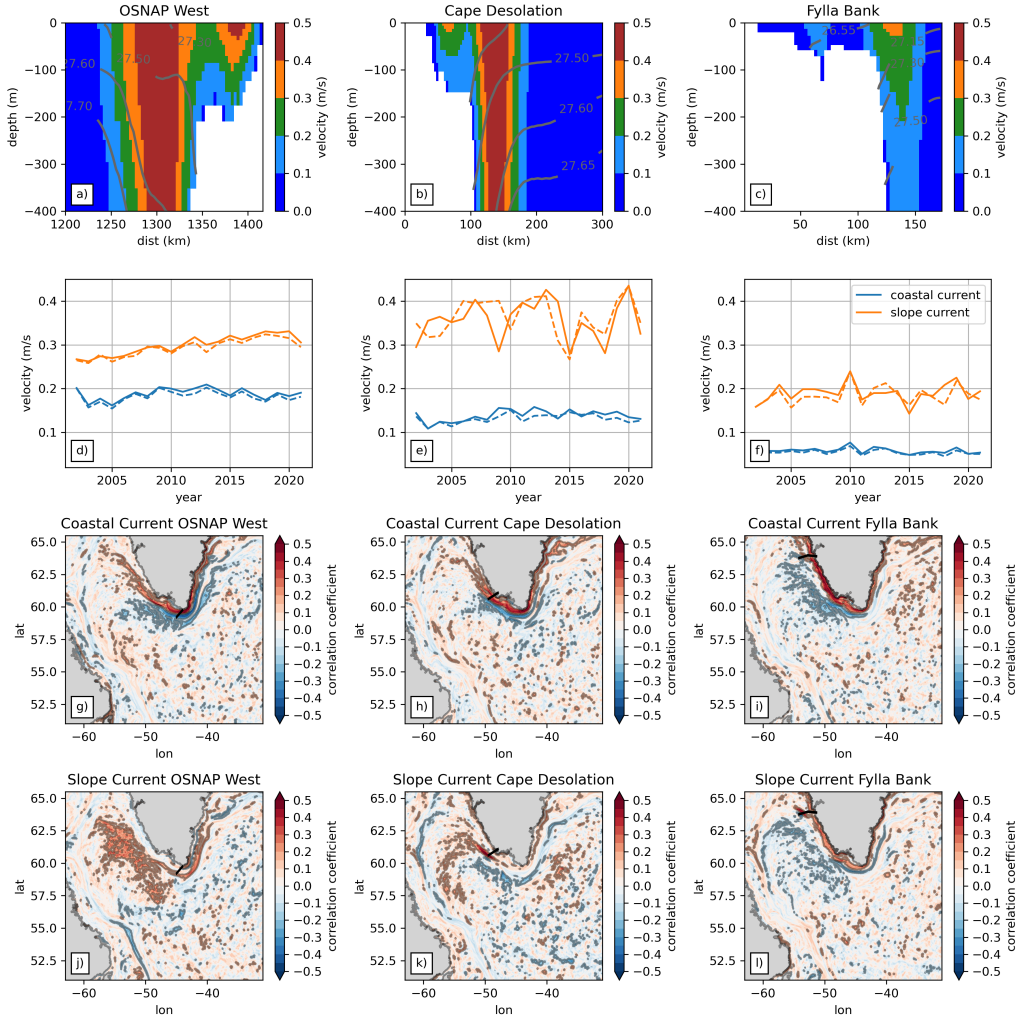
Figure S3. (a) Mean (2002–2021) current velocity magnitude at OSNAP West. (b) Cape Desolation. (c) Fylla Bank. Gray contours indicate the isopycnals referenced to the surface. (d) The annual mean current speed depth averaged the over the top 200 m for the coastal (blue) and slope current (orange) for OSNAP West. Solid lines depict REF and dashed ones SENS. (e) Cape Desolation. (f) Fylla Bank. (g) Correlation between the coastal current velocity at OSNAP West and the horizontal surface density gradient. The gray contour indicates significant areas based on the 1st and 99th confidence intervals. The black line shows the specified cross section along the shelf. The light gray contours indicate the west Greenland shelf and eddy shedding region. (h) Correlation at Cape Desolation. (i) Fylla Bank. (j) The correlation between slope current velocity and the surface density gradient at OSNAP West. (k) Cape Desolation. (l) Fylla Bank.

Text S4

We compute the stratification percent changes in REF due to the increase in Greenland freshwater fluxes with respect to the stratification in SENS for the winters (January–March) of 2009 and 2012 (Figures S4a, c). In 2009, there is a positive percent change (increase), in stratification in REF from 58–45°W in the depth range 200–1500 m. Southeast of Cape Farewell (43–38°W), there is a negative percent change (decrease) in stratification (Figure S4a) at 200–1000 m. The MLD in the LAB is deeper for SENS than REF, but both model runs feature deep convection with the MLD reaching depths greater than $z_{critical} = 1000$ m. From 48–38°W REF has a slightly shallower MLD but around a depth of $z_{critical}$. The MLD becomes shallower up to depths of 500 m east of 38°W. In support of the argument about Greenland-sourced freshwater being entrained at different depths in REF and SENS by the deep convection in the LAB, we present passive tracer concentration percent changes in Figure S4b, d. In 2009, there is a negative percent change of meltwater tracer content between 43 and 33°W from 1000–2000 m depth in REF (red patch in Figure S4b). Especially in 2009, Greenland-sourced freshwater likely spread at greater depth into the Irminger Sea (IRM) from the LAB deep convection center.

In 2012, the decrease in stratification appears surface intensified south of Cape Farewell and then weakens but spreads further east (43–33°W) and in depth (Figure S4c). The MLD in both REF and sensitivity experiment are comparable with MLDs reaching up to 1500m in the LAB. In the IRM from 39–35°W REF has deeper MLDs with a difference of 400m compared to the SENS experiment. Less passive tracer content has spread further east and is mixed downward in 2012 (Figure S4d), with SENS containing higher amounts of Greenland meltwater there. The increase in meltwater presence coincides with the shallower MLD in SENS from 38–34°W.
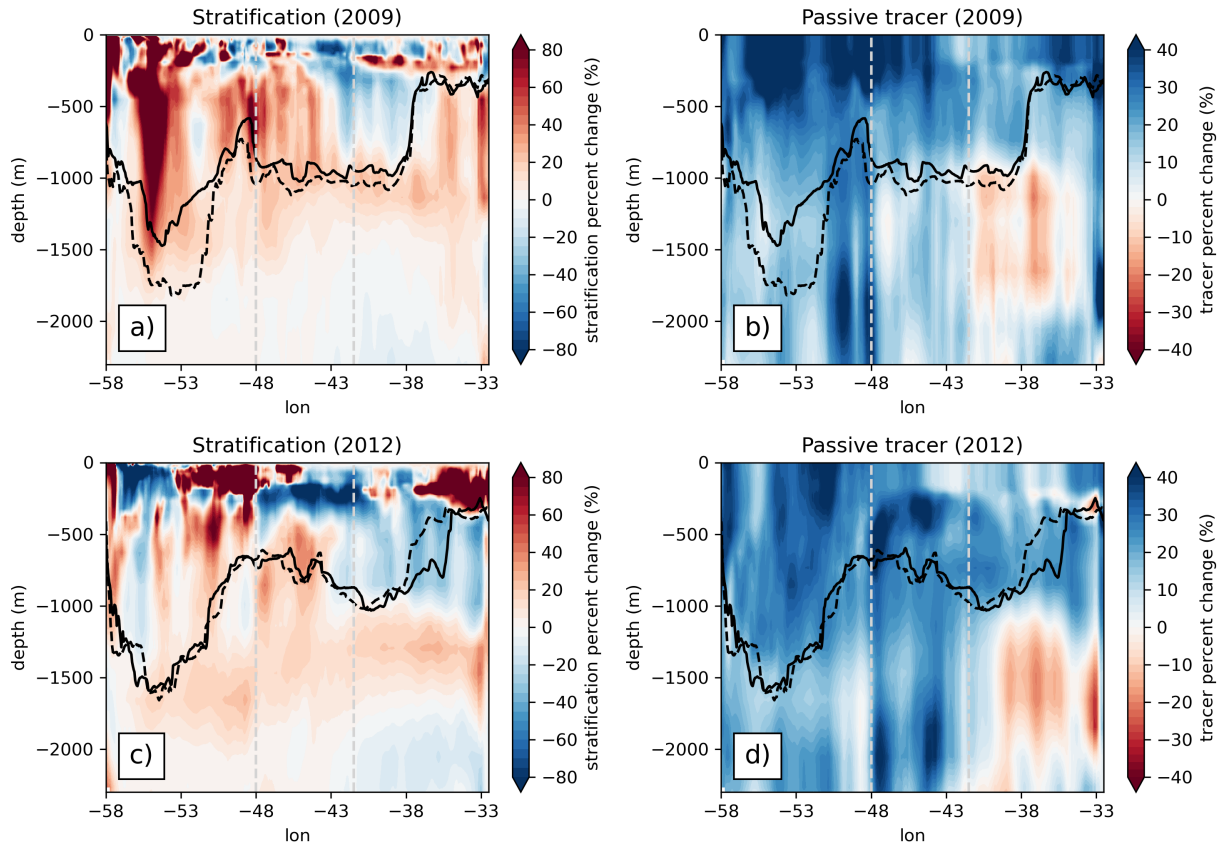
February 28, 2024, 2:28pm

:

Figure S4. (a) The percent change in winter mean stratification in 2009 between REF and SENS. The annual maximum MLD from REF is the solid black line, while the dashed line is the sensitvity. (b) The percent change of Greenland meltwater passive tracer content in winter. (c) Same as (d) but for 2012. (d) Same as (b) but for 2012. The dashed vertical gray lines indicate the separation between WEST, MID, and EAST regions.

Text S5

Convective resistance (CR) is the quantification of water column stability to a particular depth (Gillard et al., 2022; Frajka-Williams et al., 2014; Holdsworth & Myers, 2015). The CR, based on Gillard et al. (2022), for each model grid cell is defined as:

$$CR(h) = \frac{g}{\rho_0}\Big[h\sigma_0(h) - \int_0^h \sigma_0(z)dz\Big], \tag{2}$$

where g is gravity (9.8 m/s^2), ρ_0 is REF density (1026 kg/m^3), σ_0 is the potential density referenced to the surface, and h is the mixing depth. Maximum MLDs have been observed to reach depths of 2000m in the IRM (Sterl & de Jong, 2022; Zunino et al., 2020) but we choose a depth (h) of 1500 m as an upper limit of maximum MLDs in the IRM (Pickart et al., 2003). A high, positive CR indicates a stronger resistance to convection (Gillard et al., 2022; Bailey et al., 2005) and stably stratified layers, zero CR indicates mixing, and a negative CR would indicates unstable stratification (Gillard et al., 2022; Frajka-Williams et al., 2014), which is unlikely to show in monthly mean model output used here since overturning would have been simulated.

Figure S5a and b show the difference in winter mean convective resistance between REF and sensitivity for years 2009–2013 and 2015–2018. Both show higher CR in the LAB and lower values in the IRM for REF. Positive/negative values signifying greater/smaller CR in REF. In 2009–2013, it appears that the majority of negative and significant CR occur just south of the potential deep convection contour in the IRM (EAST region) (Figure S5a). There are significant positive CR changes in the eddy shedding region and southeast of Cape Farewell.

In 2015–2018 (Figure S5b), there is greater CR in REF in the central LAB and within the pDCA. The majority of negative, significant CR differences occur outside the eastern boundary

of the potential deep convection region but there is significantly lower CR in REF where the largest MLD differences occur in 2015–2018.

From 1997 onwards, CR differences start to slowly evolve as more Greenland-sourced freshwater begins to accumulate in REF than in SENS in all three regions WEST, MID, and EAST of the pDCA (Figure S5c). From about 2009 onwards, REF and SENS begin to separate. Particularly in EAST (green line), i.e. the IRM, CR systematically becomes smaller in REF thn in SENS. This underlines a role of freshwater from Greenland in decreasing CR ultimately leading to an eastward shift or expansion of the deep convection region in 2015–2018.

There is less of a systematic spread in the LAB (WEST) and south of Cape Farewell (MID) between REF and SENS. From 2011 to 2018, REF shows elevated mean winter CR than SENS. Note that MLDs in the LAB can reach to depths of 2000 m (Gillard et al., 2022; Yashayaev & Loder, 2017) and thus there may not be an imprint on CR referenced to 1500 m from the reduced deep convection discussed above. Interestingly and in agreement with an eastward shift of deep convection in 2015–2018, CR averaged over EAST reaches lower values than in WEST in both REF and SENS.
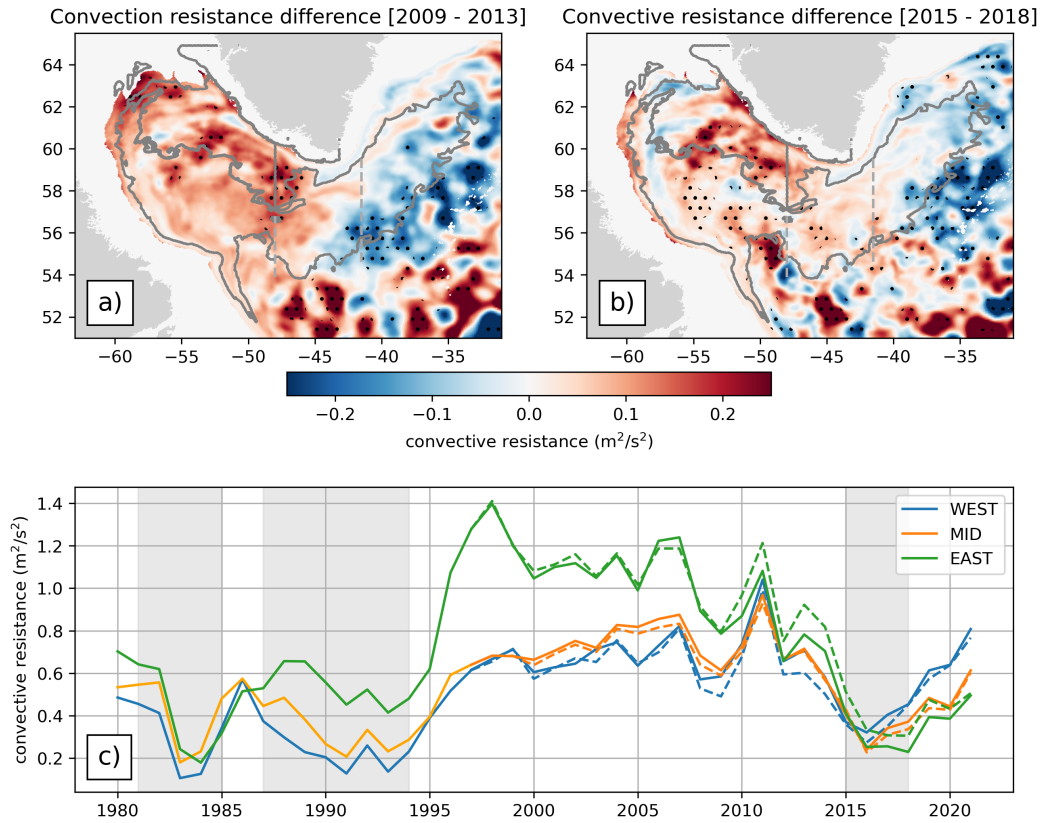
Figure S5. (a) The convective resistance difference (REF minus SENS) averaged over winter (January–March) from 2009–2013. (b) Winter convective resistance over 2015–2018. The gray contours indicate the west Greenland shelf, eddy shedding region, and pDCA. The dashed vertical, gray lines indicate the separation between WEST, MID, and EAST within the pDCA. (c) The convective resistance averaged over WEST (blue), MID (orange), and EAST (green). The solid line is a combination of the hindcast simulation (1980–1996) and REF (from 1997 onwards). The dashed line depicts SENS. The light grey vertical bars indicate associated periods of strong deep convection.

References

Bailey, D. A., Rhines, P. B., & Häkkinen, S. (2005, October). Formation and pathways of North Atlantic Deep Water in a coupled ice–ocean model of the Arctic–North Atlantic

Oceans. *Climate Dynamics*, *25*(5), 497–516. doi: 10.1007/s00382-005-0050-3

Bamber, J. L., Tedstone, A. J., King, M. D., Howat, I. M., Enderlin, E. M., van den Broeke, M. R., & Noel, B. (2018). Land Ice Freshwater Budget of the Arctic and North Atlantic Oceans: 1. Data, Methods, and Results. *Journal of Geophysical Research: Oceans*, *123*(3), 1827–1837. doi: 10.1002/2017JC013605

Biastoch, A., Schwarzkopf, F. U., Getzlaff, K., Rühs, S., Martin, T., Scheinert, M., . . . Böning, C. W. (2021, September). Regional imprints of changes in the Atlantic Meridional Overturning Circulation in the eddy-rich ocean model VIKING20X. *Ocean Science*, *17*(5), 1177–1211. doi: 10.5194/os-17-1177-2021

Castelao, R. M., Luo, H., Oliver, H., Rennermalm, A. K., Tedesco, M., Bracco, A., . . . Medeiros, P. M. (2019). Controls on the Transport of Meltwater From the Southern Greenland Ice Sheet in the Labrador Sea. *Journal of Geophysical Research: Oceans*, *124*(6), 3551–3560. doi: 10.1029/2019JC015159

Debreu, L., Vouland, C., & Blayo, E. (2008, January). AGRIF: Adaptive grid refinement in Fortran. *Computers & Geosciences*, *34*(1), 8–13. doi: 10.1016/j.cageo.2007.01.009

de Jong, M. F., & de Steur, L. (2016). Strong winter cooling over the Irminger Sea in winter 2014–2015, exceptional deep convection, and the emergence of anomalously low SST. *Geophysical Research Letters*, *43*(13), 7106–7113. doi: 10.1002/2016GL069596

Frajka-Williams, E., Rhines, P. B., & Eriksen, C. C. (2014, January). Horizontal Stratification during Deep Convection in the Labrador Sea. *Journal of Physical Oceanography*, *44*(1), 220–228. doi: 10.1175/JPO-D-13-069.1

Gillard, L. C., Hu, X., Myers, P. G., & Bamber, J. L. (2016). Meltwater pathways from marine terminating glaciers of the Greenland ice sheet. *Geophysical Research Letters*, *43*(20),

10,873–10,882. doi: 10.1002/2016GL070969

Gillard, L. C., Pennelly, C., Johnson, H. L., & Myers, P. G. (2022, March). The Effects of Atmospheric and Lateral Buoyancy Fluxes on Labrador Sea Mixed Layer Depth. *Ocean Modelling*, *171*, 101974. doi: 10.1016/j.ocemod.2022.101974

Gou, R., Feucher, C., Pennelly, C., & Myers, P. G. (2021). Seasonal cycle of the coastal west greenland current system between cape farewell and cape desolation from a very high-resolution numerical model. *Journal of Geophysical Research: Oceans*, *126*(5), e2020JC017017. doi: https://doi.org/10.1029/2020JC017017

Gou, R., Pennelly, C., & Myers, P. G. (2022). The Changing Behavior of the West Greenland Current System in a Very High-Resolution Model. *Journal of Geophysical Research: Oceans*, *127*(8), e2022JC018404. doi: 10.1029/2022JC018404

Hallberg, R. (2013, December). Using a resolution function to regulate parameterizations of oceanic mesoscale eddy effects. *Ocean Modelling*, *72*, 92–103. doi: 10.1016/j.ocemod.2013.08.007

Holdsworth, A. M., & Myers, P. G. (2015, June). The Influence of High-Frequency Atmospheric Forcing on the Circulation and Deep Convection of the Labrador Sea. *Journal of Climate*, *28*(12), 4980–4996. doi: 10.1175/JCLI-D-14-00564.1

Lozier, M. S., Li, F., Bacon, S., Bahr, F., Bower, A. S., Cunningham, S. A., . . . Zhao, J. (2019, February). A sea change in our view of overturning in the subpolar North Atlantic. *Science*, *363*(6426), 516–521. doi: 10.1126/science.aau6592

Luo, H., Castelao, R. M., Rennermalm, A. K., Tedesco, M., Bracco, A., Yager, P. L., & Mote, T. L. (2016, July). Oceanic transport of surface meltwater from the southern Greenland ice sheet. *Nature Geoscience*, *9*(7), 528–532. doi: 10.1038/ngeo2708

Madec, G. (2016). Nemo ocean engine. *Scientific notes of climate modeling center*, 406.

Mortensen, J. (2018). Report on hydrographic conditions off southwest greenland june/july 2017. *NAFO SCR Doc*, *18*(005), 8.

Myers, P. G., Donnelly, C., & Ribergaard, M. H. (2009, January). Structure and variability of the West Greenland Current in Summer derived from 6 repeat standard sections. *Progress in Oceanography*, *80*(1), 93–112. doi: 10.1016/j.pocean.2008.12.003

Pacini, A., & Pickart, R. S. (2022, January). Meanders of the West Greenland Current near Cape Farewell. *Deep Sea Research Part I: Oceanographic Research Papers*, *179*, 103664. doi: 10.1016/j.dsr.2021.103664

Pickart, R. S., Straneo, F., & Moore, G. W. K. (2003, January). Is Labrador Sea Water formed in the Irminger basin? *Deep Sea Research Part I: Oceanographic Research Papers*, *50*(1), 23–52. doi: 10.1016/S0967-0637(02)00134-6

Piron, A., Thierry, V., Mercier, H., & Caniaux, G. (2016, March). Argo float observations of basin-scale deep convection in the Irminger sea during winter 2011–2012. *Deep Sea Research Part I: Oceanographic Research Papers*, *109*, 76–90. doi: 10.1016/j.dsr.2015.12.012

Piron, A., Thierry, V., Mercier, H., & Caniaux, G. (2017). Gyre-scale deep convection in the subpolar North Atlantic Ocean during winter 2014–2015. *Geophysical Research Letters*, *44*(3), 1439–1447. doi: 10.1002/2016GL071895

Rühs, S., Oliver, E. C. J., Biastoch, A., Böning, C. W., Dowd, M., Getzlaff, K., . . . Myers, P. G. (2021). Changing Spatial Patterns of Deep Convection in the Subpolar North Atlantic. *Journal of Geophysical Research: Oceans*, *126*(7), e2021JC017245. doi: 10.1029/2021JC017245

Schiller-Weiss, I., Martin, T., Karstensen, J., & Biastoch, A. (2023). Do Salinity Variations Along the East Greenland Shelf Show Imprints of Increasing Meltwa-

ter Runoff? *Journal of Geophysical Research: Oceans*, *128*(10), e2023JC019890. (_eprint: https://onlinelibrary.wiley.com/doi/pdf/10.1029/2023JC019890) doi: 10.1029/ 2023JC019890

Slater, T., Shepherd, A., McMillan, M., Leeson, A., Gilbert, L., Muir, A., ... Briggs, K. (2021, November). Increased variability in Greenland Ice Sheet runoff from satellite observations. *Nature Communications*, *12*(1), 6069. (Number: 1 Publisher: Nature Publishing Group) doi: 10.1038/s41467-021-26229-4

Sterl, M. F., & de Jong, M. F. (2022). Restratification Structure and Processes in the Irminger Sea. *Journal of Geophysical Research: Oceans*, *127*(12), e2022JC019126. doi: 10.1029/ 2022JC019126

Stolzenberger, S., Rietbroek, R., Wekerle, C., Uebbing, B., & Kusche, J. (2022). Simulated Signatures of Greenland Melting in the North Atlantic: A Model Comparison With Argo Floats, Satellite Observations, and Ocean Reanalysis. *Journal of Geophysical Research: Oceans*, *127*(11), e2022JC018528. doi: 10.1029/2022JC018528

Tedesco, M., Fettweis, X., Van den Broeke, M., Wal, R., Smeets, P., Berg, W., ... Box, J. (2011, January). The role of albedo and accumulation in the 2010 melting record in Greenland. *Environmental Research Letters*, *6*, 014005. doi: 10.1088/1748-9326/6/1/014005

Tsujino, H., Urakawa, S., Nakano, H., Small, R. J., Kim, W. M., Yeager, S. G., ... Yamazaki, D. (2018, October). JRA-55 based surface dataset for driving ocean–sea-ice models (JRA55-do). *Ocean Modelling*, *130*, 79–139. doi: 10.1016/j.ocemod.2018.07.002

Yashayaev, I., & Loder, J. W. (2017). Further intensification of deep convection in the Labrador Sea in 2016. *Geophysical Research Letters*, *44*(3), 1429–1438. doi: 10.1002/2016GL071668

Zunino, P., Mercier, H., & Thierry, V. (2020, January). Why did deep convection persist over

four consecutive winters (2015–2018) southeast of Cape Farewell? *Ocean Science*, *16*(1), 99–113. doi: 10.5194/os-16-99-2020